Phase Transitions
Vol. 83, Nos. 10–11, October–November 2010, 931–941

Taylor & Francis
Taylor & Francis Group

THz and infrared studies of multiferroic hexagonal $Y_{1-x}Eu_xMnO_3$ (x=0–0.2) ceramics

V. Goian[a], S. Kamba[a]*, C. Kadlec[a], D. Nuzhnyy[a], P. Kužel[a], J. Agostinho Moreira[b], A. Almeida[b] and P.B. Tavares[c]

[a]*Institute of Physics, ASCR, Na Slovance 2, 18221 Prague 8, Czech Republic;* [b]*Departamento de Física da Faculdade de Ciências, IFIMUP, Universidade do Porto, Rua do Campo Alegre, 687, 4169-007, Porto, Portugal;* [c]*Centro de Química de Vila Real, Universidade de Trás-os-Montes e Alto Douro, Apartado 1013, 5001-801, Vila Real, Portugal*

(*Received 24 May 2010; final version received 28 June 2010*)

We report an investigation of hexagonal $Y_{1-x}Eu_xMnO_3$ ceramics with $x = 0$, 0.1, and 0.2 using infrared (IR) and terahertz (THz) spectroscopies in the temperature range between 5 and 900 K. The temperature dependence of the THz permittivity reveals a kink near the antiferromagnetic (AFM) phase transition temperature $T_N \approx 70$ K, giving evidence of a strong spin–lattice coupling. Below T_N, two absorption peaks were revealed in the THz spectra close to 43 and 73 cm^{-1}. While the first peak corresponds to a sharp AFM resonance exhibiting softening on heating towards T_N, the second one may be attributed to an impurity mode or a multiphonon absorption peak. High-temperature THz spectra measured up to 900 K reveal only small gradual increase of the permittivity in agreement with a weak phonon softening observed in the IR reflectance spectra upon heating. This corresponds to an improper ferroelectric character of the phase transition proposed from first principle calculations by Fennie and Rabe (Phys. Rev. B 72: 100103(R), 2005).

Keywords: multiferroics; lattice dynamics; phonons; phase transitions

1. Introduction

Multiferroic rare-earth manganites $RMnO_3$ (R = rare earth) are materials which are studied intensively for their pronounced coupling between magnetization and ferroelectric (FE) polarization (magnetoelectric effect) [1], which can be used in technological applications like non-volatile memories [2], magnetic sensors or FE-gate field-effect transistors [3]. The rare-earth manganites exist in two crystallographic forms: manganites with a relatively small rare-earth ionic radius crystallize to form a hexagonal structure, while manganites with a larger ionic radius of the rare earth elements are orthorhombic with MnO_6 octahedra forming the perovskite structure. The hexagonal manganites are characterized by MnO_5 bipyramids which form layers in the ***a*–*b*** plane. Along the ***c*** direction, the layers of MnO_5 are well separated by rare earth elements [4].

*Corresponding author. Email: kamba@fzu.cz

ISSN 0141–1594 print/ISSN 1029–0338 online

DOI: 10.1080/01411594.2010.509603
http://www.informaworld.com

One of the most intensively studied manganites is hexagonal $YMnO_3$, although yttrium does not belong to rare earth ions. $YMnO_3$ is a high-temperature FE (T_C near 940 K) [5] and it becomes AFM below 70 K [6,7]. It crystallizes in the space group $P6_3/mmc$ (D^4_{6h}, $Z=2$) in the high-temperature paraelectric phase [8] and it transforms to the polar space group $P6_3cm$ (C^3_{6v}, $Z=6$) in the FE phase below ~940 K [9]. The absence of large Born effective charges and the polarization obtained by a buckling of layered MnO_5 bipyramids, accompanied by off-centered displacements of Y and in-plane O ions, have been referred to as geometrical ferroelectricity [4]. The polarization was found to be rather high, around 5 $\mu C\,cm^{-2}$ [10]. The magnetic order is given by a frustrated triangular basal plane spin structure [11]. Nènert et al. [12] revealed a new intermediate phase between 1125 and 1350 K in a single crystal of $YMnO_3$ using dilatometry and differential thermal analysis. The existence of the intermediate phase is still under debate, but on the other hand there is relatively large spread of published T_C values in literature from 913 to 1270 K [9]. Fennie and Rabe [13] made the first principle calculations and came to the conclusion that the intermediate phase is energetically less favorable than a single improper FE phase transition. According to them, the FE phase transition is caused by a softening of optic phonon at the Brillouin zone boundary with $q=(1/3, 1/3, 0)$, and spontaneous polarization arises from the coupling of this phonon to a zone center mode. If this is true, no pronounced dielectric anomaly is expected near T_C. However, direct dielectric measurements are missing near T_C due to a rather high conductivity above room temperature. We found just one old conference paper [5] about dielectric studies of $YMnO_3$ performed at 150 MHz up to 1050 K showing a relatively small permittivity peak and large dielectric loss near 910 K.

In contrast to hexagonal $YMnO_3$, the ferroelectricity in orthorhombic-$RMnO_3$ occurs below the magnetic phase transition (typically below 40 K) due to locking of the incommensurate helicoidal spin structure to a commensurate one leading to the creation of transverse polarization as a consequence of interaction between the spins. Due to such spin-induced ferroelectricity, the magneto–electric coupling is very large in the orthorhombic $RMnO_3$ [14].

In the case of hexagonal $YMnO_3$, the magneto–electric coupling has a different origin. Linear magnetoelectric coupling is forbidden by symmetry, but it was shown that the AFM domain walls strongly interact with the lattice strain in FE domain walls due to the piezomagnetic effect [1,15]; so any switching of FE polarization triggers flipping of the AFM order parameter. Very recently, Choi et al. [16] discovered that the FE domain walls and structural antiphase boundaries are mutually locked and this strong locking leads to an incomplete poling even under a high electric field.

In hexagonal $YMnO_3$, the spin–phonon coupling is anomalously large. This was demonstrated in X-ray diffraction studies [17], dielectric permittivity [18,19], thermal conductivity [20], and in inelastic neutron scattering studies [21]. Infrared (IR) [22] and Raman scattering spectra [23] revealed a pronounced phonon hardening near and below T_N due to spin–lattice coupling, which is responsible for the decrease of dielectric permittivity [19] near T_N.

Inelastic neutron scattering revealed three magnon branches. Two of them are degenerate near the BZ center and have frequencies near 40 cm^{-1} [24,25]. The AFM resonance was confirmed at the same frequency by means of FIR spectroscopy [26]. Recent polarized inelastic neutron scattering studies revealed that the excitation seen at 1.5 K near 40 cm^{-1} has a hybrid character of magnetic spin wave and a lattice vibration [27]. In other words, it should contribute to both magnetic permeability and dielectric permittivity. The authors proposed to explain this mode hybridization by Dzyaloshinskii–Moriya interaction [27].

In this article, we report on terahertz (THz) and IR studies of hexagonal $Y_{1-x}Eu_xMnO_3$ ($x = 0, 0.1$, and 0.2) ceramics. Temperature and Eu concentration dependence of AFM resonance observed near 40 cm^{-1} was determined. The IR reflectivity studies of $YMnO_3$ single crystal below 300 K have been recently published [22]. In this article, we extend these investigations up to 900 K, i.e., close to the FE phase transition; in addition, our IR data are complemented by THz measurements for more accurate determination of the permittivity up to 900 K. Based on our data, we confirm the improper FE character of the phase transition, as recently proposed by Fennie and Rabe [13].

2. Experimental details

High-quality $Y_{1-x}Eu_xMnO_3$ ceramics were prepared by the sol–gel urea combustion method. A detailed study of $EuMnO_3$ and $GdMnO_3$ ceramics prepared in this way has led to results very similar to those obtained for the corresponding single crystals [28]. The valence of the europium ion was checked through XPS technique, and no evidences for other valences than the Eu(III) could be detected. As the samples were fast cooled from 1350°C down to room temperature, significant deviations of the oxygen occupancy are not expected, excluding the existence of significant amounts of Mn(IV) ions [29].

IR transmission and reflectivity measurements were performed using a Fourier Transform IR Spectrometer Bruker IFS 113v in the temperature range of 5–900 K and frequency range between 15 and 3000 cm^{-1} (0.45–90 THz) with the resolution of 2 cm^{-1}. A helium-cooled Si bolometer operating at 1.6 K was used as a detector for low-temperature measurements, while a pyroelectric doped triglycine sulfate (DTGS) detector was used above room temperature. Time-domain THz spectroscopy measurements were performed in the range of 100 GHz and 2 THz. Linearly polarized THz probing pulses were generated using a Ti:sapphire femtosecond laser whose pulses iluminated an interdigitated photoconducting GaAs switch. THz signal was detected using the electro–optic sampling with 1-mm thick [1 1 0] ZnTe crystal. A continuous flow helium cryostat from Optistat CF Oxford Instruments was used for cooling the samples down to 10 K and a commercial high-temperature cell Specac P/N 5850 was used for heating of samples up to 900 K in both IR and THz spectrometers.

The plane-parallel samples were polished on both sides to obtain a mirror-like surface. The thickness and diameter of all $Y_{1-x}Eu_xMnO_3$ ceramic samples were 1.032 and 9 mm, respectively.

3. Results and discussion

Figure 1 shows the IR reflectivity spectra of $YMnO_3$ between 10 and 900 K. Spectra are plotted only below 700 cm^{-1}, because the spectra at higher frequencies are temperature independent. Spectra of $Y_{1-x}Eu_xMnO_3$ ceramics (not shown here) are very similar to those of $YMnO_3$. A gradual decrease of reflection band intensities with increasing temperature is seen. This is caused by an increase of the phonon damping with temperature, as will be discussed below. Parameters of the observed phonons were obtained from the fits. The reflectivity spectra $R(\omega)$ are related to spectra of the complex index of refraction $n^*(\omega)$ using the relation

$$R(\omega) = \left|\frac{n^*(\omega) - 1}{n^*(\omega) + 1}\right|^2 \quad (1)$$

where $n^*(\omega) = \sqrt{\varepsilon^*(\omega)\mu^*(\omega)}$.

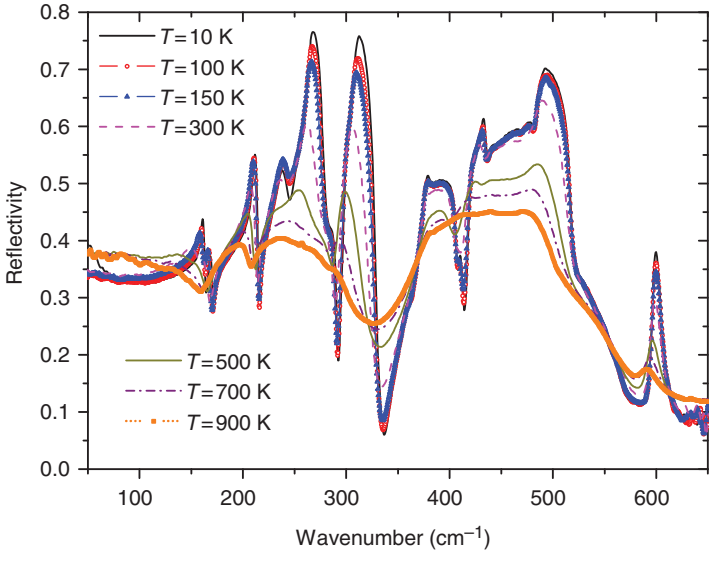

Figure 1. Temperature dependence of the IR reflectivity spectra of $YMnO_3$ ceramics.

The complex magnetic permeability $\mu^*(\omega) = \mu'(\omega) + i\mu''(\omega)$ exhibits usually no dispersion in the THz spectra of dielectrics; so $\mu'(\omega) = 1$ and $\mu''(\omega) = 0$ and thus $n^*(\omega) = \sqrt{\varepsilon^*(\omega)}$ in non-magnetic materials. However, in our AFM material some magnetic excitation can appear in the THz or IR spectra and since we cannot unambiguously distinguish between magnetic and dielectric excitations from our spectra of ceramics, we will systematically plot the real and imaginary parts of the product $\varepsilon^*(\omega)\mu^*(\omega)$ spectra.

The complex permittivity $\varepsilon^*(\omega)$ is in our model described by a sum of classical damped quasiharmonic oscillators

$$\varepsilon^*(\omega) = \varepsilon_\infty + \sum_{j=1}^{n} \frac{\Delta\varepsilon_{\mathrm{TO}j}\omega_{\mathrm{TO}j}^2}{\omega_{\mathrm{TO}j}^2 - \omega^2 + i\omega\gamma_{\mathrm{TO}j}} \tag{2}$$

where $\omega_{\mathrm{TO}j}$, $\Delta\varepsilon_{\mathrm{TO}j}$, and $\gamma_{\mathrm{TO}j}$ are the eigenfrequency, dielectric strength, and damping of the jth polar phonon, respectively. The high-frequency permittivity, due to electronic absorption processes in the visible and UV ranges is ε_∞. The static permittivity $\varepsilon(0)$ is given by

$$\varepsilon(0) = \sum_{j=1}^{n} \Delta\varepsilon_{\mathrm{TO}j} + \varepsilon_\infty. \tag{3}$$

We note that in classical displacive FEs, where no dispersion exists below the phonon frequencies, $\varepsilon(0)$ usually corresponds to the low-frequency permittivity measured in radiofrequency range. We also note that magnetic permeability spectra $\mu^*(\omega)$ can be fitted as well with a harmonic oscillator model similar to Equation (2).

The low-frequency part (below $100\,\mathrm{cm}^{-1}$) of our far-infrared (FIR) spectra was actually investigated by means of three independent techniques: FIR reflectivity (Figure 1), FIR transmission (Figure 2), and time-domain THz transmission spectroscopy, which gives directly the real and imaginary parts of the product $\varepsilon^*(\omega)\mu^*(\omega)$ (Figure 3). All these

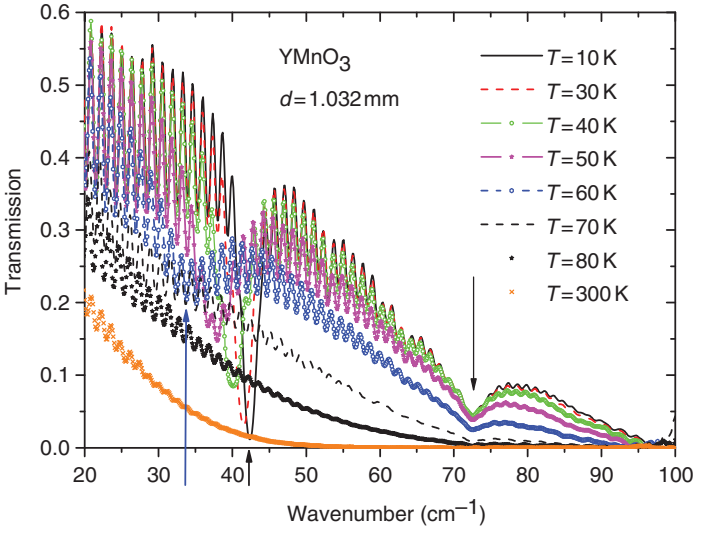

Figure 2. FIR transmission spectra at various temperatures. Two absorption anomalies are clearly observed around 40 and 73 cm^{-1}.

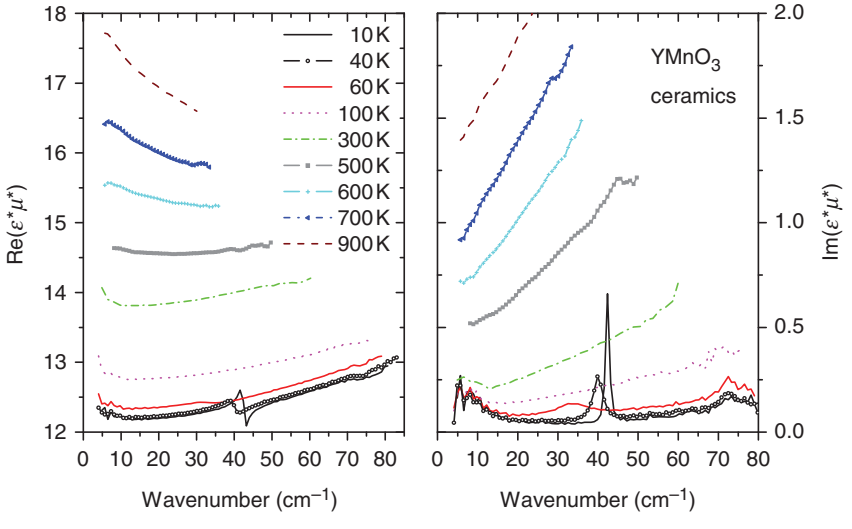

Figure 3. Temperature dependence of real and imaginary parts of experimental THz spectra of the product $\varepsilon^*\mu^*$ in a broad temperature range. The spin wave near 40 cm^{-1} is clearly seen; a weaker excitation near 73 cm^{-1} is also apparent – see also FIR transmission spectra in Figure 2.

spectra were fitted simultaneously and the obtained complex spectra are shown in Figure 4.

A sharp resonant peak is seen near 40 cm^{-1} in Figures 2 and 3. This is the AFM resonance which was briefly described in reference [26]. The AFM resonance causes dispersion only in $\mu^*(\omega)$ spectra and its frequency decreases on heating toward T_N (Figure 5). Similar AFM resonances with slightly lower frequencies were observed also in $Y_{1-x}Eu_xMnO_3$ ceramics ($x = 0.1$ and 0.2).

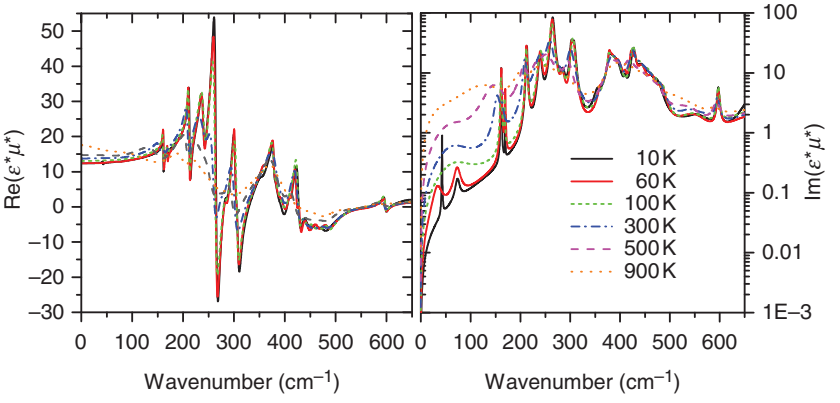

Figure 4. Real and imaginary parts of $\varepsilon^*\mu^*$ in $YMnO_3$ ceramics at various temperatures obtained from the simultaneous fit of THz and FIR spectra. Peaks in the imaginary part correspond to the phonon and magnon frequencies.

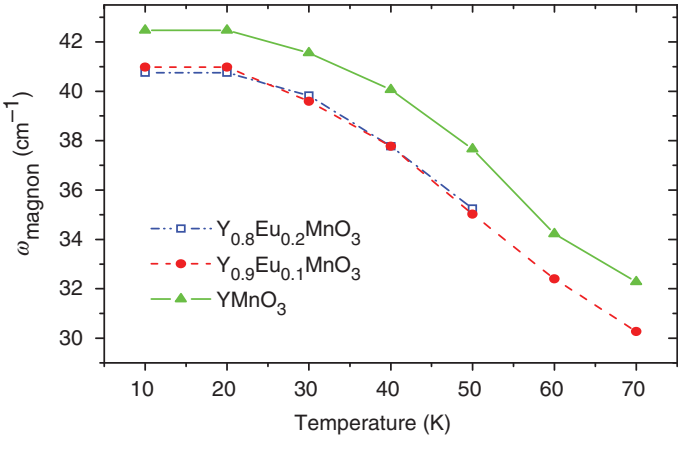

Figure 5. Temperature dependence of the AFM resonance frequencies in the $Y_{1-x}Eu_xMnO_3$ ceramics for $x = 0, 0.1$, and 0.2.

Phonon frequencies obtained from the fits of IR reflectivity exhibit no dramatic change with temperature; only a small gradual decrease of their values was observed (Figure 6). This phonon softening will be explained below.

Polarized IR reflectivity spectra of a $YMnO_3$ single crystal were published by Zaghrioui et al. [22]. Nine A_1 and fourteen E_1-symmetry polar modes are allowed from the factor group analysis [30] for the electric vector **E** of the IR beam parallel and perpendicular to the ***c*** crystal axis, respectively. Zaghrioui et al. [22] observed seven A_1 modes and eight E_1 modes. Our spectra of ceramics shown in Figure 1 are unpolarized; therefore we see a mixture of both polarized spectra; especially above 350 cm^{-1}, the modes are highly overlapped and it is very difficult to distinguish all the modes in the reflectivity spectra. In spite of this, we used 24 oscillators for the fits of the spectra at 10 K (including one magnon), which exactly correspond to the number of polar phonons expected from the factor group analysis [30]. Ten polar-mode frequencies are similar to frequencies

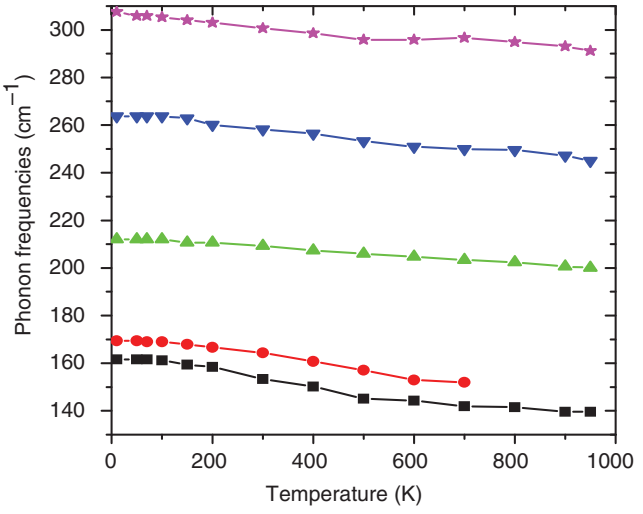

Figure 6. Temperature dependence of the selected phonon frequencies in the $YMnO_3$ ceramics.

observed in the single crystal [22]; however the rest of the modes have slightly different frequencies, because the fit of ceramics describes a mixture of A_1 and E_1 spectra and the effective mode frequencies in ceramics can be shifted from the A_1 and E_1 mode frequencies. Figure 6 shows the frequencies of phonons which exhibit some relatively stronger temperature dependences. Other modes, which are not plotted in Figure 6, have the following frequencies (in cm^{-1}) at 10 K: 73.8, 239.5, 284.8, 302.2, 354.4, 378.2, 382.8, 394.7, 410.3, 426.7, 442.3, 457.9, 472.5, 477.1, 555.0, 597.1, and 666.7. The small decrease of phonon frequencies observed on heating in Figure 6 is mainly due to thermal expansion with increasing temperature. The phonon damping increases with rising temperature as well; therefore the intensity of reflectivity bands in Figure 1 decreases at high temperatures.

The THz spectra taken above T_N are just the complex permittivity spectra, because the AFM resonance contributing to $\mu^*(\omega)$ spectra is seen only below T_N. One can see that the real part of permittivity (ε') increases on heating, so that the static permittivity $\varepsilon'(0)$ increases from 12.5 (at 10 K) to 17.8 (at 900 K). Such a change is rather small and is caused by the small phonon softening seen in Figure 6. In the case of proper FE phase transition, $\varepsilon'(0)$ should increase on heating toward T_C, according to the Curie–Weiss law. Our observation of only small permittivity increase on heating supports the improper character of the FE phase transition originally suggested by Fennie and Rabe [13]. In this case, the FE phase transition is driven by a soft phonon from the Brillouin zone boundary with $\mathbf{q} = (1/3, 1/3, 0)$, which does not contribute to permittivity above T_C. It can contribute to $\varepsilon'(0)$ only in the FE phase, but dielectric strength of this newly IR-activated mode is usually very small; so the change of $\varepsilon'(0)$ with temperature is also very weak. A small change of THz permittivity near T_C can be expected also in the case of an order–disorder phase transition, but in this case some larger structural disorder should be seen in paraelectric phase, which is not the case [8,9].

In the literature, there are several reports about an intermediate phase between FE and paraelectric phases [8,12,31]. Fennie and Rabe [13] have shown, based on symmetry analysis, that the intermediate phase, if it exists, should be paraelectric $P6_3/mcm$ ($Z = 6$). It means that the FE phase transition should be a proper FE driven by a zone–center polar

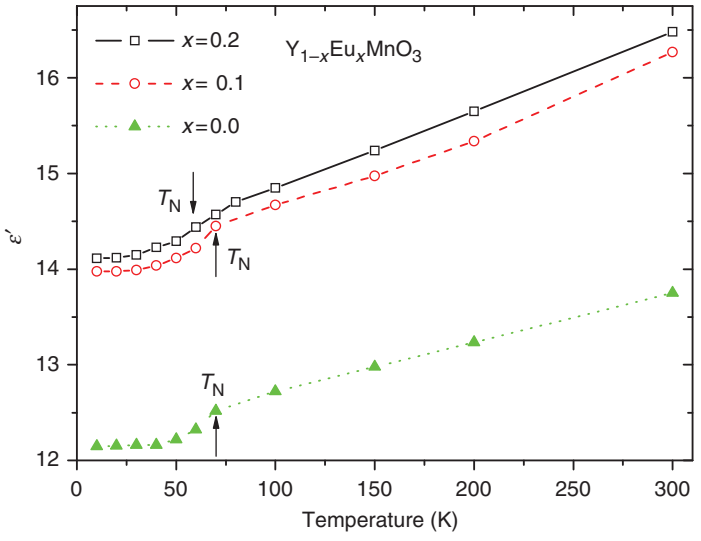

Figure 7. Temperature dependence of ε' in the Y_{1-x} Eu_xMnO_3 ($x = 0, 0.1$, and 0.2) ceramics at 0.5 THz from THz spectra. Lines are guides for the eyes.

soft mode and a large dielectric anomaly at T_C should be expected. Fennie and Rabe have shown that this scenario is energetically less probable than the improper FE phase transition and our small experimental permittivity seen 40 K below T_C really supports the improper character of it. Nevertheless, one must also admit, that the small permittivity increase could also occur due to T_C much higher than 900 K. This is less probable, but some experimental papers [8,12] reported it.

FIR transmission (Figure 2) and THz spectra (Figure 3) reveal sharp resonant absorptions near 40 cm^{-1} in the AFM phase of $YMnO_3$. This is the AFM resonance which was briefly reported in [26] and its frequency corresponds also to the zone center magnon seen in INS spectra [21,24,25,27]. The same AFM resonance was revealed also in the THz spectra of $Y_{1-x}Eu_xMnO_3$ with $x = 0.1$ and 0.2; the frequency is slightly lower than that for $YMnO_3$ (Figure 5).

Another sharp absorption is seen in the FIR transmission spectra near 73 cm^{-1} (Figure 2). A hint of this is also seen in the THz spectra (Figure 3). Unfortunately, it can be revealed only at low temperatures below 60 K, i.e., in the AFM phase, because the sample is not transparent at higher temperatures. From these data, it is not clear whether this excitation is of magnon or polar origin. This mode is not seen in IR reflectivity spectra, because its dielectric strength is very small ($\Delta\varepsilon \approx 0.1$). However, for careful simultaneous fit of IR reflectivity and higher temperature THz spectra, this heavily damped mode is also needed at higher temperatures up to 900 K. Its existence in the paramagnetic phase gives evidence that the mode is not of magnetic origin. We stress that without this mode it is impossible to fit the enhanced THz dielectric losses in Figure 3. The mode can be seen in Figure 4 as a broad loss maximum below 100 cm^{-1}. Oscillator strength of this mode increases on heating, which is not typical of one phonon absorption, but is possible in a multiphonon absorption. Nevertheless, multiphonon excitation should die out on cooling. In our case, we see this mode down to 10 K, which gives more evidence for some defect origin of this mode. This assumption is also supported by our preliminary IR transmission and THz spectra of $YMnO_3$ single crystal, where this mode was not observed.

Temperature dependence of the permittivity obtained in $Y_{1-x}Eu_xMnO_3$ at 0.5 THz shows a small drop down near T_N (Figure 7), which is a consequence of large spin–lattice coupling responsible for an isostructural phase transition at T_N and large atomic displacements revealed in the XRD studies [17]. The spin–lattice coupling causes hardening of some phonons near T_N, especially of the E_1-symmetry mode observed in the IR spectra of single crystal [22]. Similar dielectric anomaly was observed in the 1 MHz data published in [19] with a slightly higher value of ε'. This was probably caused by higher density of ceramics investigated in [19]. Temperature, where the drop down in ε' appears, can be used for a rough estimation of T_N. One can see that T_N is approximately the same in $Y_{1-x}Eu_xMnO_3$ for $x = 0$, 0.1 and 0.2 (around 70k as usually reported in the literature). Nevertheless, in $x = 0.2$ sample the dielectric anomaly is more smeared than in the rest of the ceramics, giving evidence of broadening of the AFM phase transitian with Eu substitution.

4. Conclusions

High-temperature IR reflectivity spectra of $YMnO_3$ reveal only a small gradual decrease of several phonon frequencies, which is responsible for an observed small increase of the THz permittivity on heating toward 900 K. Such phonon and dielectric behaviors support the improper character of the FE phase transition near 940 K connected with a tripling of the unit cell and soft mode anomaly at the Brillouin zone boundary. Our experimental data support theoretical predictions of Fennie and Rabe [13] and do not confirm the existence of an intermediate paraelectric phase with tripled unit cell above T_C experimentally revealed in papers [8,12]. The apparent intermediate phase is probably caused by defects and related to the diffuse character of the phase transition.

Sharp AFM resonance and softening of its frequency on heating toward T_N were revealed in the THz spectra. Strong spin–phonon coupling is demonstrated by a remarkable decrease of THz permittivity near T_N. Eu-substituted $YMnO_3$ exhibits similar magnon and dielectric properties as $YMnO_3$.

Acknowledgements

This study was supported by Fundação para a Ciência e Tecnologia, through the Project PTDC/CTM/67575/2006, and by Programme Alban, the European Union Programme of High Level Scholarships for Latin America (Scholarship no. E06D100894BR). This study was also supported by the Czech Science Foundation (Project 202/09/0682), SVV-2010-261303, and AVOZ 10100520. The authors thank J. Petzelt for critical reading of the manuscript.

References

[1] M. Fiebig, Th. Lottermoser, D. Frohlich, A.V. Goltsev, and R.V. Pisarev, *Observation of coupled magnetic and electric domains*, Nature 419 (2002), pp. 818–820.

[2] N. Fujimura, T. Ishida, T. Yoshimura, and T. Ito, *Epitaxially grown $YMnO_3$ film: New candidate for nonvolatile memories devices*, Appl. Phys. Lett. 69 (1996), pp. 1011–1013.

[3] D. Ito, N. Fujimura, T. Yoshimura, and T. Ito, *Ferroelectric properties of $YMnO_3$ epitaxial films for ferroelectric-gate field effect transistors*, J. Appl. Phys. 93 (2003), pp. 5563–5567.

[4] B.B. van Aken, T.T.M. Palstra, A. Filippetti, and N. Spaldin, *The origin of ferroelectricity in magnetoelectric $YMnO_3$*, Nat. Mater. 3 (2004), pp. 164–170.

[5] Ph. Coeure, P. Guinet, J.C. Peuzin, G. Buisson, and E.F. Bertaut, *Ferroelectric properties of hexagonal orthomanganites of Yttrium and rare earths*, in *Proceedings of International Meeting on*

Ferroelectricity, V. Dvorak, A. Fouskova, and P. Glogar, eds., Institute of the Czechoslovak Academy of Science, Prague, 1966, Vol. 1, pp. 332–340.

[6] E.F. Bertaut, M. Mercier, and R. Pauthenet, *Ordre magnétique et propriétés magnétiques de $MnYO_3$*, J. Phys. 25 (1964), pp. 550–557.

[7] A. Munoz, J.A. Alonso, M.J. Martinez-Lope, M.T. Casais, J.L. Martinez, and M.T. Fernandez-Diaz, *Magnetic structure of hexagonal $RMnO_3$ ($R = Y$, Sc): Thermal evolution from neutron powder diffraction data*, Phys. Rev. B, 62 (2000), pp. 9498–9510.

[8] K. Lukaszewicz and J. Karut-Kalicinska, *X-ray investigations of the crystal structure and phase transitions of $YMnO_3$*, Ferroelectrics 7, (1974), pp. 81–82.

[9] S.C. Abrahams, *Ferroelectricity and structure in the $YMnO_3$ family*, Acta Crystallogr., Sect. B: Struct. Sci. 57 (2001), pp. 485–490.

[10] G.A. Smolenskii and V.A. Bokov, *Coexistence of magnetic and electric ordering in crystals*, J. Appl. Phys. 35 (1964), pp. 915–918.

[11] E.F Bertaut and M. Mercier, *Structure magnetique de $MnYO_3$*, Phys. Lett. 5 (1963), pp. 27–29.

[12] G. Nénert, M. Pollet, S. Marinel, G.R. Blake, A. Meetsma, and T.T.M. Palstra, *Experimental evidence for an intermediate phase in multiferroic $YMnO_3$''*, J. Phys. Condens. Matter. 19 (2007), p. 466212.

[13] C. Fennie and K.M. Rabe, *Ferroelectric transitions in $YMnO_3$ from first principles*, Phys. Rev. B, 72 (2005), p. 100103 R.

[14] T. Kimura, *Spiral Magnets as Magnetoelectrics*, Annu. Rev. Mater. Res. 37 (2007), pp. 387–413.

[15] A.V. Goltsev, R.V. Pisarev, Th. Lottermoser, and M. Fiebig, *Structure and interaction of antiferromagnetic domain walls in hexagonal $YMnO_3$*, Phys. Rev. Lett. 90, (2003), p. 177204.

[16] T. Choi, Y. Horibe, H.T. Yi, Y.J. Choi, W. Wei, and S.-W. Cheong, *Insulating interlocked ferroelectric and structural antiphase domain walls in multiferroic $YMnO_3$*, Nat. Mater. 9 (2010), pp. 253–258.

[17] S. Lee, A. Pirogov, M. Kang, K.-H. Jang, M. Yonemura, T. Kamiyama, S.-W. Cheong, F. Gozzo, N. Shin, H. Kimura, Y. Noda, and J.-G. Park, *Giant magneto elastic coupling in multiferroic hexagonal manganites*, Nature, 451 (2008), pp. 805–809.

[18] N. Iwata and K. Kohn, *Dielectric anomalies at magnetic transitions of hexagonal rare earth manganese oxides $RMnO_3$*, J. Phys. Soc. Jpn 67 (1998), pp. 3318–3319.

[19] D.G. Tomuta, S. Ramakrishnan, G.J. Nieuwenhuys, and J.A. Mydosh, *The magnetic susceptibility, specific heat and dielectric constant of hexagonal $YMnO_3$, $LuMnO_3$ and $ScMnO_3$*, J. Phys. Condens. Matter. 13 (2001), pp. 4543–4552.

[20] P.A. Sharma, J.S. Ahn, N. Hur, S. Park, S.B. Kim, S. Lee, J.-G. Park, S. Guha, and S.-W. Cheong, *Thermal conductivity of geometrically frustrated, ferroelectric $YMnO_3$: Extraordinary spin-phonon interactions*, Phys. Rev. Lett. 93 (2004), p. 177202.

[21] S. Petit, F. Moussa, M. Hennion, S. Pailhès, L. Pinsard-Gaudart, and A. Ivanov, *Spin phonon coupling in hexagonal multiferroic $YMnO_3$*, Phys. Rev. Lett. 99 (2007), p. 266604.

[22] M. Zaghrioui, V. TaPhuoc, R.A. Souza, and M. Gervais, *Polarized reflectivity and lattice dynamics of multiferroic $YMnO_3$*, Phys. Rev. B, 78 (2008), p. 184305.

[23] H. Fukumura, S. Matsui, H. Harima, K. Kisoda, T. Takahashi, T. Yoshimura, and N. Fujimura, *Raman scattering studies on multiferroic $YMnO_3$*, J. Phys. Condens. Matter. 19 (2007), p. 365239.

[24] T. Chatterji, S. Ghosh, A. Singh, L.P. Regnault, and M. Rheinstädter, *Spin dynamics of $YMnO_3$ studied via inelastic neutron scattering and the anisotropic Hubbard model*, Phys. Rev. B, 76 (2007), p. 144406.

[25] T.J. Sato, S.-H. Lee, T. Katsufuji, M. Masaki, S. Park, J.R.D. Copley, and H. Takagi, *Unconventional spin fluctuations in the hexagonal antiferromagnet $YMnO_3$*, Phys. Rev. B, 68 (2003), p. 014432.

[26] T Penney, P. Berger, and K. Kritiyakirana, *Far infrared antiferromangetic resonance in hexagonal $YMnO_3$*, J. Appl. Phys., 40 (1969), pp. 1234–1235.

[27] S. Pailhes, X. Fabreges, L.P. Regnault, L. Pinsard-Godart, L. Mirebau, F. Moussa, M. Hennion, and S. Petit, *Hybrid Goldstone modes in multiferroic $YMnO_3$ studied by polarized inelastic scattering*, Phys. Rev. B, 79 (2009), p. 134409.

[28] W.S. Ferreira, J. Agostinho Moreira, A. Almeida, M.R. Chaves, J.P. Araújo, J.B. Oliveira, J.M. Machado Da Silva, M.A. Sá, T.M. Mendonça, P. Simeão Carvalho, J. Kreisel, J.L. Ribeiro, L.G. Vieira, P.B. Tavares, and S. Mendonça, *Spin-phonon coupling and magnetoelectric properties: $EuMnO_3$ versus $GdMnO_3$*, Phys. Rev. B, 79 (2009), p. 054303.

[29] J.A. Alonso, M.J. Martínez-Lope, M.T. Casais, and M.T. Fernández-Díaz, *Evolution of the Jahn–Teller distortion of MnO_6 octahedra in $RMnO_3$ Perovskites ($R = Pr, Nd, Dy, Tb, Ho, Er, Y$): A neutron diffraction study*, Inorg. Chem. 39 (2000), pp. 917–923.

[30] M.N. Iliev, H.-G. Lee, V.N. Popov, M.V. Abrashev, A. Hamed, R.L. Meng, and C.W. Chu, *Raman- and infrared-active phonons in hexagonal $YMnO_3$: Experiment and lattice-dynamical calculations*, Phys. Rev. B, 56 (1997), pp. 2488–2494.

[31] Th. Lonkai, D.G. Tomuta, U. Amann, J. Ihringer, R.W.A. Hendrikx, D.M. Többens, and J.A. Mydosh, *Development of the high-temperature phase of hexagonal manganites*, Phys. Rev. B, 69 (2004), p. 134108.